

# Gyrokinetic particle simulations of reversed shear Alfvén eigenmode excited by antenna and fast ions

Wenjun Deng,<sup>1</sup> Zhihong Lin,<sup>1,2,a)</sup> Ihor Holod,<sup>1</sup> Xin Wang,<sup>1,3</sup> Yong Xiao,<sup>1</sup> and Wenlu Zhang<sup>1,4</sup>

<sup>1</sup>*Department of Physics and Astronomy, University of California, Irvine, California 92697, USA*

<sup>2</sup>*Fusion Simulation Center, Peking University, Beijing 100871, China*

<sup>3</sup>*Institute of Fusion Theory and Simulation, Zhejiang University, Hangzhou, Zhejiang 310027, China*

<sup>4</sup>*CAS Key Laboratory of Basic Plasma Physics, University of Science and Technology of China, Hefei, Anhui 230026, China*

(Received 2 July 2010; accepted 12 September 2010; published online 9 November 2010)

Global gyrokinetic particle simulations of reversed shear Alfvén eigenmode (RSAE) have been successfully performed and verified. We have excited the RSAE by initial perturbation, by external antenna, and by energetic ions. The RSAE excitation by antenna provides verifications of the mode structure, the frequency, and the damping rate. When the kinetic effects of the background plasma are artificially suppressed, the mode amplitude shows a near-linear growth. With kinetic thermal ions, the mode amplitude eventually saturates due to the thermal ion damping. The damping rates measured from the antenna excitation and from the initial perturbation simulation agree very well. The RSAE excited by fast ions shows an exponential growth. The finite Larmor radius effects of the fast ions are found to significantly reduce the growth rate. With kinetic thermal ions and electron pressure, the mode frequency increases due to the elevation of the Alfvén continuum by the geodesic compressibility. The nonperturbative contributions from the fast ions and kinetic thermal ions modify the mode structure relative to the ideal magnetohydrodynamic (MHD) theory. The gyrokinetic simulations have been benchmarked with extended hybrid MHD-gyrokinetic simulations. © 2010 American Institute of Physics. [doi:10.1063/1.3496057]

## I. INTRODUCTION

Generated by heating sources or fusion products, energetic particles exhibit distinct behavior, which is a crucial problem for plasmas in future tokamaks such as ITER, and is therefore being widely studied. These energetic particles can drive unstable shear Alfvén waves, e.g., the toroidal Alfvén eigenmode<sup>1</sup> (TAE) and the reversed shear Alfvén eigenmode (RSAE) (a.k.a. the Alfvén cascade),<sup>2</sup> and can excite nonperturbative modes called the energetic particle mode (EPM).<sup>3</sup>

The RSAE has been observed in JT-60U,<sup>4</sup> the Joint European Torus (JET),<sup>5</sup> the Tokamak Fusion Test Reactor,<sup>6</sup> Alcator C-Mod,<sup>7</sup> D-IIID,<sup>8</sup> and the National Spherical Torus Experiment<sup>9</sup> reversed shear tokamaks. It can be excited by not only energetic particles, but also the Alfvénic ion temperature gradient mechanism.<sup>10–13</sup> A variety of phenomena about the RSAE have been seen, an important one being the “grand cascade”:<sup>5</sup> when  $q_{\min}$  passes a low-order rational number, particularly an integer, RSAEs near the  $q_{\min}$  surface with the same frequency but different  $n$  and  $m$  harmonics are excited simultaneously. This phenomenon provides a method to measure the time when  $q_{\min}$  hits a low-order rational number<sup>5,14</sup> and the location of the rational  $q_{\min}$  surface.<sup>15</sup> This method is routinely used in tokamak experiments, especially for the internal transport barrier diagnosis.<sup>16–20</sup> Second harmonic generation of the RSAE has been observed in the experiment<sup>7</sup> and interpreted by an magnetohydrodynamics (MHD) theory.<sup>21</sup> The RSAE can have interactions with the

TAE, such as the coupling between these two modes<sup>22</sup> and the theoretically predicted<sup>23,24</sup> transition from RSAE to TAE.<sup>25</sup> Large mode amplitude and energetic particle loss are observed during the transition.<sup>25</sup> Electron cyclotron heating is observed to be able to stabilize the RSAE and reduce the energetic particle transport.<sup>26</sup>

The earliest linear RSAE theory based on ideal MHD (Ref. 2) has been extended to include various effects, such as toroidicity,<sup>24</sup> ellipticity and triangularity,<sup>27</sup> finite pressure,<sup>28,29</sup> pressure gradient,<sup>30,31</sup> and finite Larmor radius (FLR) effects.<sup>32,33</sup> Kinetic interactions between the RSAE and the background plasma, as well as the energetic particles are also theoretically studied.<sup>13,23,34</sup> Numerical simulations<sup>27,31,35</sup> have recovered many linear properties seen in experiments and theories. Hybrid MHD-gyrokinetic code (HMGC) simulations<sup>23,36</sup> have observed nonlinear saturation of the RSAE causing enhanced energetic particle transport, which are the only nonlinear simulations of the RSAE reported so far.

Although many linear properties of the RSAE have been reported, understanding of the linear and nonlinear background plasma particle kinetic effects<sup>13,34</sup> on the RSAE remains inadequate. Global, fully self-consistent, and nonlinear kinetic simulations are needed to predict the linear stability boundaries and the nonlinear saturation amplitude of the shear Alfvén waves. Many recent gyrokinetic simulations<sup>37–42</sup> are on the TAE and none is on the RSAE. Here, we would like to study the linear and nonlinear properties of the RSAE, with the thermal particle kinetic effects, using the global gyrokinetic particle code GTC.<sup>43</sup> The current GTC version<sup>44</sup> has new features such as full- $f$  and  $\delta f$

<sup>a)</sup>Author to whom correspondence should be addressed. Electronic mail: zhihongli@uci.edu.

simulation, general geometry using experimental equilibrium data, kinetic electrons, and electromagnetic simulation.<sup>45,46</sup> GTC has recently been applied to study microturbulence properties in reversed shear plasmas,<sup>47</sup> transport of energetic particles by microturbulence,<sup>48</sup> and beta-induced Alfvén eigenmode in tokamaks.<sup>49</sup> In the current work, we have successfully excited the RSAE by initial perturbation, by external antenna, and by fast ions. The RSAE excitation by antenna provides verifications of the mode structure, the frequency, and the damping rate. When the kinetic effects of the background plasma are artificially suppressed, the mode amplitude shows a near-linear growth. With kinetic thermal ions, the mode amplitude eventually saturates due to the thermal ion damping. The damping rates measured from the antenna excitation and from the initial perturbation simulation agree very well. Such a damping rate measurement technique has been used in JET.<sup>50,51</sup> The RSAE excited by fast ions shows an exponential growth. The finite Larmor radius effects of the fast ions are found to significantly reduce the growth rate. With kinetic thermal ions and electron pressure, the mode frequency increases due to the elevation of the Alfvén continuum by the geodesic compressibility. The non-perturbative contributions from the fast ions and kinetic thermal ions modify the mode structure relative to the ideal MHD theory. The gyrokinetic simulations have been benchmarked with extended hybrid MHD-gyrokinetic (XHMGC)<sup>52,53</sup> simulations.

This paper is organized as follows: the gyrokinetic simulation model is described in Sec. II, the antenna excitation results and the fast ion excitation results are presented in Secs. III and IV, respectively, and Sec. V summarizes this work.

## II. GYROKINETIC SIMULATION MODEL

In this section, we first describe our electromagnetic gyrokinetic formulation in GTC. Then we show that when kinetic effects are artificially turned off, the formulation is reduced to the ideal MHD theory. Finally, we derive a model RSAE dispersion relation from the reduced equation.

### A. Formulation for gyrokinetic simulation

In this paper, we call the regular ion species the thermal ion and the energetic ion species the fast ion. Both ion species are described by the nonlinear gyrokinetic equation<sup>54</sup> to resolve the spatial scale on the order of  $k_{\perp}\rho_{i,f} \sim 1$ ,

$$(\partial_t + \dot{\mathbf{X}} \cdot \nabla + \dot{v}_{\parallel} \partial_{v_{\parallel}}) f_{\alpha}(\mathbf{X}, \mu, v_{\parallel}, t) = 0, \quad (1)$$

$$\dot{\mathbf{X}} = v_{\parallel} \frac{\mathbf{B}}{B_0} + \mathbf{v}_E + \mathbf{v}_c + \mathbf{v}_g, \quad (2)$$

$$\dot{v}_{\parallel} = -\frac{1}{m_{\alpha} B_0} \mathbf{B}^* \cdot (\mu \nabla B_0 + Z_{\alpha} \nabla \phi) - \frac{Z_{\alpha}}{m_{\alpha} c} \partial_t A_{\parallel}, \quad (3)$$

where subscripts  $\alpha = e, i, f$  stand for the particle species, electron  $e$ , thermal ion  $i$ , or fast ion  $f$ ;  $Z_{\alpha}$ ,  $m_{\alpha}$ , and  $\Omega_{\alpha}$  are the electric charge, mass, and cyclotron frequency, respectively;

the magnetic field  $\mathbf{B}$  is separated into the equilibrium part  $\mathbf{B}_0$  and the perturbed part  $\delta\mathbf{B}$ , so  $\mathbf{B} = \mathbf{B}_0 + \delta\mathbf{B}$ ;  $\mathbf{B}^*$  is given by

$$\mathbf{B}^* = \mathbf{B}_0 + \frac{B_0 v_{\parallel}}{\Omega_{\alpha}} \nabla \times \mathbf{b}_0 + \delta\mathbf{B}. \quad (4)$$

The  $\mathbf{E} \times \mathbf{B}$  drift velocity  $\mathbf{v}_E$ , the magnetic curvature drift velocity  $\mathbf{v}_c$ , and the grad- $\mathbf{B}$  drift velocity are, respectively, given by

$$\mathbf{v}_E = \frac{c \mathbf{b}_0 \times \nabla \phi}{B_0}, \quad (5)$$

$$\mathbf{v}_c = \frac{v_{\parallel}^2}{\Omega_{\alpha}} \nabla \times \mathbf{b}_0, \quad (6)$$

$$\mathbf{v}_g = \frac{\mu}{m_{\alpha} \Omega_{\alpha}} \mathbf{b}_0 \times \nabla B_0. \quad (7)$$

Electrons are simulated using the electromagnetic fluid-kinetic hybrid electron model,<sup>38,44,55,56</sup> which is built on the expansion of the electron response into the lowest-order adiabatic part and a higher-order kinetic response based on the small electron-ion mass ratio. With this fluid-kinetic hybrid electron model, the nonresonant current is fully retained in the fluid equations with no need to resolve the dynamics of these nonresonant electrons. Meanwhile, the dynamics of the electron resonances and the nonadiabatic response of magnetically trapped electrons are recovered by the higher-order kinetic corrections. In this paper, only the adiabatic part is used and electrons are described by the linear fluid continuity equation. Extension of the continuity equation to include kinetic electron response and nonlinearity is straightforward and has been published for simulations of microturbulence.<sup>45</sup> The continuity equation is obtained by integrating the gyrokinetic equation Eq. (1) in the linear drift-kinetic limit for electrons assuming  $k_{\perp}\rho_e \ll 1$  and ignoring equilibrium current<sup>44</sup>

$$\begin{aligned} \partial_t \delta n_e + \mathbf{B}_0 \cdot \nabla \left( \frac{n_{e0} \delta u_{e\parallel}}{B_0} \right) + B_0 \mathbf{v}_E \cdot \nabla \left( \frac{n_{e0}}{B_0} \right) \\ - n_{e0} (\mathbf{v}_{e*} + \mathbf{v}_E) \cdot \frac{\nabla B_0}{B_0} = 0, \end{aligned} \quad (8)$$

where  $\mathbf{v}_{e*} = c \mathbf{b}_0 \times \nabla (\delta P_{e\parallel} + \delta P_{e\perp}) / (n_{e0} e B_0)$ ,  $\delta P_{e\parallel} = \int m v_{\parallel}^2 \delta f_e d\mathbf{v}$ , and  $\delta P_{e\perp} = \int \mu B_0 \delta f_e d\mathbf{v}$ . For a uniform background plasma, in the lowest order,  $\delta P_{e\parallel}$  and  $\delta P_{e\perp}$  can be expressed as

$$\delta P_{e\parallel} = \delta P_{e\perp} = n_{e0} e \delta \phi_{\text{eff}}, \quad (9)$$

where  $\delta \phi_{\text{eff}}$  is the effective potential representing the parallel electric field

$$\delta E_{\parallel} = -\mathbf{b}_0 \cdot \nabla \delta \phi_{\text{eff}}. \quad (10)$$

As the background plasma is uniform, in the lowest order,  $\delta \phi_{\text{eff}}$  is found by

$$\frac{e \delta \phi_{\text{eff}}}{T_e} = \frac{\delta n_e}{n_{e0}}. \quad (11)$$

The electrostatic potential  $\delta\phi$  is described by the gyrokinetic Poisson's equation<sup>57</sup>

$$\frac{Z_i^2 n_i}{T_i} (\delta\phi - \delta\tilde{\phi}) = \sum_{\alpha=e,i,f} Z_\alpha \delta n_\alpha \quad (12)$$

and the vector potential  $\delta\mathbf{A}$  by the gyrokinetic Ampère's law

$$\frac{c}{4\pi} \{\nabla \times [\nabla \times (\delta A_{\parallel} \mathbf{b}_0)] \cdot \mathbf{b}_0\} \mathbf{b}_0 = \sum_{\alpha=e,i,f} \delta \mathbf{J}_{\alpha\parallel} \quad (13)$$

Here  $\delta\mathbf{B}_{\parallel}=0$  is assumed, so  $\delta\mathbf{A}$  has only parallel component  $\delta A_{\parallel}$ . Define an inductive potential

$$\delta\phi_{\text{ind}} = \delta\phi_{\text{eff}} - \delta\phi. \quad (14)$$

Noticing that  $\delta E_{\parallel} = -\mathbf{b}_0 \cdot \nabla \delta\phi - \partial_t \delta A_{\parallel} / c$  and using Eq. (10), we have

$$\partial_t \delta A_{\parallel} = c \mathbf{b}_0 \cdot \nabla \delta\phi_{\text{ind}}. \quad (15)$$

An optional antenna is implemented through an external potential perturbation in  $\delta\phi_{\text{ind}}$ . When the antenna is turned on,  $\delta\phi_{\text{ind}}$  becomes

$$\delta\phi_{\text{ind}} = \delta\phi_{\text{eff}} - \delta\phi + \delta\phi_{\text{ant}}, \quad (16)$$

where  $\delta\phi_{\text{ant}}$  is the external potential perturbation from an optional antenna. Magnetic coordinates, which are the poloidal magnetic flux function  $\psi$ , toroidal angle  $\zeta$ , and poloidal angle  $\theta$ , are used in the GTC code. For RSAE, the antenna is implemented in this single- $n$  and single- $m$  form

$$\delta\phi_{\text{ant}} = \delta\hat{\phi}_{\text{ant}}(\psi) \cos(n_{\text{ant}}\zeta - m_{\text{ant}}\theta) \cos(\omega_{\text{ant}}t). \quad (17)$$

## B. Reduction of gyrokinetic formulation to ideal MHD theory

In this subsection, we show that with the kinetic effects turned off and in the long wavelength limit, the gyrokinetic formulation is reduced to the ideal MHD theory. Therefore, the fluid-kinetic hybrid electron model is a superset of the ideal MHD theory. The substitutions for linear normal mode theory ( $\partial_t \rightarrow -i\omega$ ,  $\mathbf{b}_0 \cdot \nabla \rightarrow ik_{\parallel}$ ) will be applied in the following derivation.

Using the same method for obtaining the electron continuity equation Eq. (8), we can obtain the continuity equation for all three particle species

$$\begin{aligned} \partial_t \delta n_\alpha + \mathbf{B}_0 \cdot \nabla \left( \frac{n_{\alpha 0} \delta u_{\alpha\parallel}}{B_0} \right) + B_0 \mathbf{v}_E \cdot \nabla \left( \frac{n_{\alpha 0}}{B_0} \right) \\ - n_{\alpha 0} (\mathbf{v}_{\alpha*} + \mathbf{v}_E) \cdot \frac{\nabla B_0}{B_0} = 0, \end{aligned} \quad (18)$$

where  $\mathbf{v}_{\alpha*} = c \mathbf{b}_0 \times \nabla (\delta P_{\alpha\parallel} + \delta P_{\alpha\perp}) / (n_{\alpha 0} Z_\alpha B_0)$ ,  $\delta P_{\alpha\parallel} = \int m v_{\parallel}^2 \delta f_{\alpha} d\mathbf{v}$ , and  $\delta P_{\alpha\perp} = \int \mu B_0 \delta f_{\alpha} d\mathbf{v}$ . This equation can be reformed to be

$$\begin{aligned} -i\omega Z_\alpha \delta n_\alpha + \nabla \cdot \delta \mathbf{J}_{\alpha\parallel} = Z_\alpha \mathbf{v}_E \cdot \left( 2n_{\alpha 0} \frac{\nabla B_0}{B_0} - \nabla n_{\alpha 0} \right) \\ - \frac{c \mathbf{b}_0 \times \nabla B_0}{B_0^2} \cdot \nabla (\delta P_{\alpha\parallel} + \delta P_{\alpha\perp}) \\ \approx Z_\alpha \mathbf{v}_E \cdot \left( 2n_{\alpha 0} \frac{\nabla B_0}{B_0} - \nabla n_{\alpha 0} \right) \\ - c \nabla \cdot \left( \frac{\mathbf{b}_0}{B_0} \times \nabla \cdot \delta \mathbf{P}_\alpha \right), \end{aligned} \quad (19)$$

where the pressure tensor is diagonal:  $\delta \mathbf{P}_\alpha = \delta P_{\alpha\parallel} \mathbf{b}_0 \mathbf{b}_0 + \delta P_{\alpha\perp} (1 - \mathbf{b}_0 \mathbf{b}_0)$  in the drift-kinetic limit and terms on the order of  $O((\epsilon/q)^2)$  are omitted, i.e.,  $\mathbf{B}_0$  is approximated to be curl-free.

As we are approaching the ideal MHD limit, the parallel electric field is ignored so  $\delta\phi_{\text{eff}}=0$ . Combining Eqs. (14) and (15), we get

$$\partial_t \delta A_{\parallel} = -c \mathbf{b}_0 \cdot \nabla \delta\phi. \quad (20)$$

In the long wavelength limit, the gyrokinetic Poisson's equation Eq. (12) becomes

$$\nabla_{\perp} \cdot \left( \frac{1}{v_A^2} \nabla_{\perp} \delta\phi \right) = -\frac{4\pi}{c^2} \sum_{\alpha=e,i,f} Z_\alpha \delta n_\alpha. \quad (21)$$

Combining this equation, gyrokinetic Ampère's law Eqs. (13) and (20), we get

$$\begin{aligned} \omega^2 \nabla_{\perp} \cdot \left( \frac{1}{v_A^2} \nabla_{\perp} \delta\phi \right) - i \mathbf{B}_0 \cdot \nabla \left\{ \frac{\nabla \times [\nabla \times (k_{\parallel} \delta\phi \mathbf{b}_0)] \cdot \mathbf{b}_0}{B_0} \right\} \\ + \frac{i4\pi\omega}{c^2} \sum_{\alpha=e,i,f} (-i\omega Z_\alpha \delta n_\alpha + \nabla \cdot \delta \mathbf{J}_{\alpha\parallel}) = 0. \end{aligned} \quad (22)$$

Plugging Eq. (19) into Eq. (22), considering charge neutrality  $\sum_{\alpha} Z_\alpha n_{\alpha 0} = 0$ , we get

$$\begin{aligned} \omega^2 \nabla_{\perp} \cdot \left( \frac{1}{v_A^2} \nabla_{\perp} \delta\phi \right) - i \mathbf{B}_0 \cdot \nabla \left\{ \frac{\nabla \times [\nabla \times (k_{\parallel} \delta\phi \mathbf{b}_0)] \cdot \mathbf{b}_0}{B_0} \right\} \\ - \frac{i4\pi\omega}{c} \nabla \cdot \left( \frac{\mathbf{b}_0}{B_0} \times \nabla \cdot \delta \mathbf{P} \right) = 0, \end{aligned} \quad (23)$$

where  $\delta \mathbf{P} = \sum_{\alpha} \delta \mathbf{P}_\alpha$  is the total perturbed pressure. Equation (23) recovers the limiting case of the ideal MHD equations in Refs. 52 and 58 except that the parallel equilibrium current is absent in this limiting model.

## C. Simplified model for RSAE dispersion relation

The RSAE is an Alfvén eigenmode with a frequency near the local extremum of the Alfvén continuum and can be derived<sup>2</sup> from Eq. (23).

In the toroidal geometry, consider only one  $n$  and  $m$  harmonic  $\delta\phi(r, \zeta, \theta) = \delta\hat{\phi}(r) \exp[i(n\zeta - m\theta)]$  and treat the toroidal coupling effect as a small correction. Dropping terms of order  $O((\epsilon/q)^2)$ , Eq. (23) becomes

$$\frac{1}{r} \frac{d}{dr} \left( r \Lambda \frac{d}{dr} \delta \hat{\phi} \right) - \frac{m^2}{r^2} \Lambda \delta \hat{\phi} - \frac{D}{r} \delta \hat{\phi} = 0, \quad (24)$$

where

$$\Lambda = \frac{\omega^2}{v_A^2} - k_{\parallel}^2, \quad (25)$$

$D$  represents contributions from the fast ion pressure, background plasma pressure gradient, toroidal coupling, magnetic shear, etc. It is apparent that Eq. (24) becomes singular when  $\Lambda=0$ , which gives the Alfvén continuum.

With a reversed shear  $q$ -profile ( $q$ -profile has an off-axis minimum  $q_{\min}$ ),  $k_{\parallel}^2=(n-m/q)^2/R^2$  has a local extremum at the  $q_{\min}$  flux surface and thus can be expanded as

$$k_{\parallel}^2 \approx (k_{\parallel}^2)_0 + \frac{1}{2} (k_{\parallel}^2)''_0 (r-r_0)^2, \quad (26)$$

where the prime symbol (') denotes the radial derivative  $d/dr$ , the subscript 0 denotes the value taken at the  $q_{\min}$  surface, and the coefficients here are related to  $q_{\min}$  by

$$(k_{\parallel}^2)_0 = \frac{1}{R^2} \left( n - \frac{m}{q_{\min}} \right)^2, \quad (27)$$

$$(k_{\parallel}^2)''_0 = \frac{2}{R^2} \left( n - \frac{m}{q_{\min}} \right) \frac{m q_{\min}''}{q_{\min}^2}. \quad (28)$$

Then Eq. (24) becomes

$$\frac{d}{dx} \left[ (x+1)(\hat{\Lambda}_0 + x^2) \frac{d}{dx} \delta \hat{\phi} \right] - \frac{m^2}{x+1} (\hat{\Lambda}_0 + x^2) \delta \hat{\phi} + Q \delta \hat{\phi} = 0, \quad (29)$$

where

$$Q = \frac{D}{\frac{1}{2} (k_{\parallel}^2)''_0 r_0} = Q_f + Q_p + Q_t + Q_s, \quad (30)$$

$x=(r-r_0)/r_0$  is the normalized radial variable,  $\hat{\Lambda}_0=[\omega^2/v_A^2 - (k_{\parallel}^2)_0]/[-\frac{1}{2}(k_{\parallel}^2)''_0 r_0^2]$  is the normalized eigenfrequency,  $Q$  is the normalization of  $D$ ,  $Q_f$  is from the fast ion contribution,<sup>2</sup>  $Q_p$  is from the background plasma pressure gradient effect,<sup>29-31</sup>  $Q_t$  is from the toroidal coupling effect,<sup>23,24</sup> and  $Q_s$  is from the magnetic shear effect. The parallel equilibrium current needs to be considered in order to calculate  $Q_s$  accurately.

Equation (29) is the normalized RSAE eigenmode equation. It is a second-order ordinary differential equation with an eigenvalue variable  $\hat{\Lambda}_0$ . If  $Q$  is real, this equation can be solved numerically using shooting method so a set of eigenmode real frequencies and mode structures can be obtained. In principle, for this type of equation, if a solution exists, then there are an infinite number of eigenmodes which are the radial harmonics<sup>31</sup> labeled by an integer  $l$ . The zeroth ( $l=0$ ) and the first ( $l=1$ ) radial harmonics have been identified in a recent DIII-D experiment.<sup>59</sup>

In general,  $Q$  can be complex and the imaginary part would give each eigenmode a growth rate (imaginary part  $\gamma$  of the frequency  $\omega=\omega_r+i\gamma$ ). Furthermore, when the background plasma pressure is considered, the singularity of Eq. (24) is no longer  $\Lambda=0$ , meaning the Alfvén continuum devi-

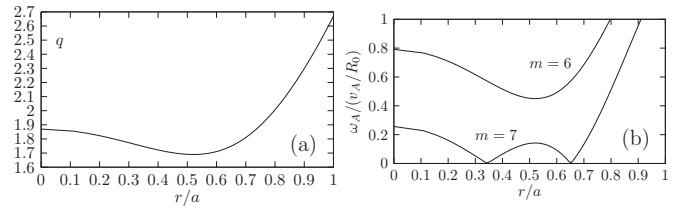


FIG. 1. (a) Safety factor  $q$ -profile. (b) Alfvén continua of  $m=6$  and  $m=7$  in ideal MHD limit and without linear coupling.

ates from  $\Lambda=0$ . The new singularity and continuum can be calculated from the MHD theory<sup>29,60</sup> or the kinetic theory.<sup>10</sup> From the kinetic theory it is given by

$$\Lambda - \left( \frac{7}{4} + \frac{T_e}{T_i} \right) \frac{2v_i^2}{v_A^2 R_0^2} = \frac{\omega^2}{v_A^2} - k_{\parallel}^2 - \left( \frac{7}{4} + \frac{T_e}{T_i} \right) \frac{2v_i^2}{v_A^2 R_0^2} = 0, \quad (31)$$

where  $v_i^2=T_e/m_i$  is the background ion thermal speed. The raise of the Alfvén continuum in Eq. (31) is due to the geodesic compressibility of thermal electrons and kinetic ions. With all these effects considered, solving the equation becomes very challenging and a computer simulation turns out to be a much easier approach to study the RSAE.

### III. ANTENNA EXCITATION OF RSAE

We use the external antenna to excite the RSAE to verify the mode structure, frequency, and damping rate in our simulations. To find the eigenmode frequency, we do multiple simulations with different antenna frequencies ( $\omega_{\text{ant}}$ ) and find out the case that has the maximum growth. The frequency of that case is the eigenmode frequency.

In our simulations, the background plasma is uniform, the inverse aspect ratio is  $a/R_0=0.335$  in a tokamak with concentric (GTC) or shifted (XHMGC) circular cross-section, and a  $q$ -profile, shown in Fig. 1(a), with  $q_{\min}=1.69$  is used. The simulations are all linear and we apply a toroidal mode filter to select only the  $n=4$  mode. Without linear coupling, the Alfvén continua of  $m=6$  and  $m=7$  in the ideal MHD limit are plotted in Fig. 1(b). Because this is the first time to use a gyrokinetic code to simulate the RSAE, we benchmark GTC results with XHMGC,<sup>52,53</sup> whose predecessor HMGC (Ref. 61) has been extensively applied to studies of the MHD modes driven by energetic particles and the EPM. XHMGC has extended HMGC to include the kinetic thermal ion effects, which are needed for our benchmark.

To recover the most basic properties of the RSAE, background plasma kinetic effects are first artificially turned off. Therefore, kinetic thermal ions are not loaded. Only the first two terms of the electron continuity equation Eq. (8) are kept as to retain quasineutrality.

Since the toroidal coupling effect is present in both GTC and XHMGC, and for the parameters used here, the toroidal coupling constant averaged over the mode width is estimated to be  $Q_{t,\text{avg}} \approx 0.35$ , which is larger than the theoretical threshold of  $1/4$ .<sup>24</sup> Therefore, eigenmodes exist no matter whether the parallel equilibrium current is present.

For the zeroth ( $l=0$ ) radial harmonic, the eigenmode frequencies found by GTC and by XHMGC are  $\omega_{\text{GTC}}$

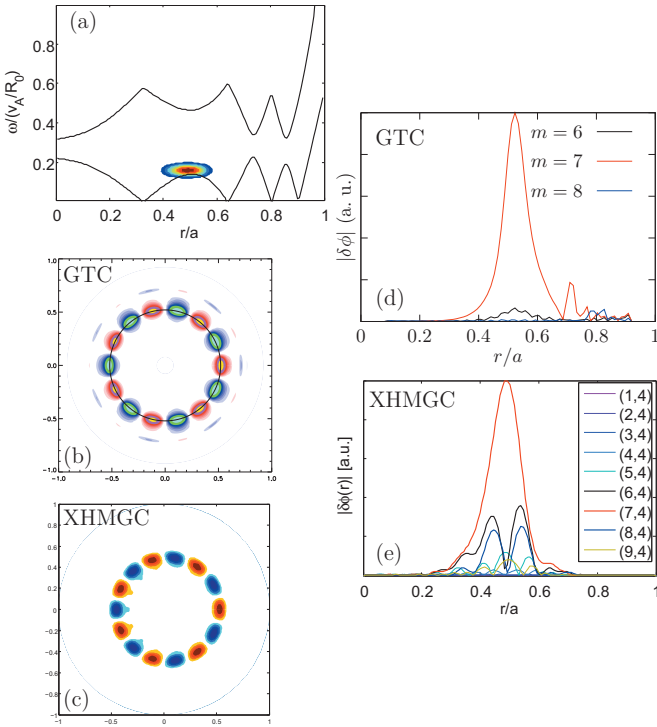


FIG. 2. (Color) Antenna excitation of  $n=4$ ,  $m=7$ , and  $l=0$  RSAE without kinetic thermal ion using GTC and XHMGC. (a) Alfvén continua and frequency spectrum from XHMGC. [(b) and (c)] Poloidal contour plots of electrostatic potential  $\delta\phi$  from GTC and XHMGC, respectively. [(d) and (e)] Radial profiles of  $\delta\phi$   $m$ -harmonics from GTC and XHMGC, respectively.

$=0.135v_A/R_0$  and  $\omega_{\text{XHMGC}}=0.160v_A/R_0$ , respectively. The mode frequency from GTC is very close to the ideal MHD accumulation point frequency  $\omega_{\text{ac}}=0.142v_A/R_0$  and is about 16% lower than that from XHMGC. This is probably due to the difference of the toroidal geometry model between the two codes, i.e., the Shafranov shift, which is on the order of  $O(\epsilon)$  and  $\epsilon=0.174$  in our simulations at the  $q_{\text{min}}$  surface. Another possible source for the difference is that the GTC simulations neglect the parallel equilibrium current, which is kept in XHMGC. The mode structures are compared in Figs. 2(b)–2(e). The dominant  $m=7$  harmonic shows similar structures in both codes. For the first ( $l=1$ ) radial harmonic, the frequency found by GTC is  $\omega=0.131v_A/R_0$ , slightly lower than the zeroth radial harmonic as expected. The mode structure is shown in Fig. 3.

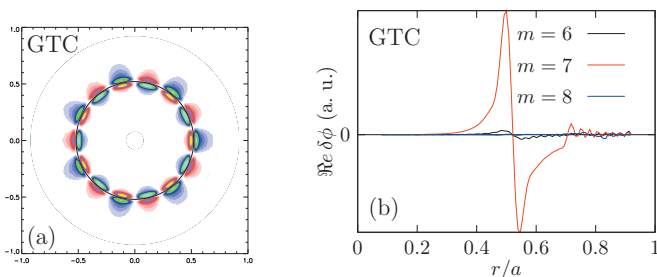


FIG. 3. (Color) Antenna excitation of  $n=4$ ,  $m=7$ , and  $l=1$  RSAE without kinetic thermal ion using GTC. (a) Poloidal contour plot of electrostatic potential  $\delta\phi$ . (b) Radial profile of  $\delta\phi$   $m$ -harmonics.

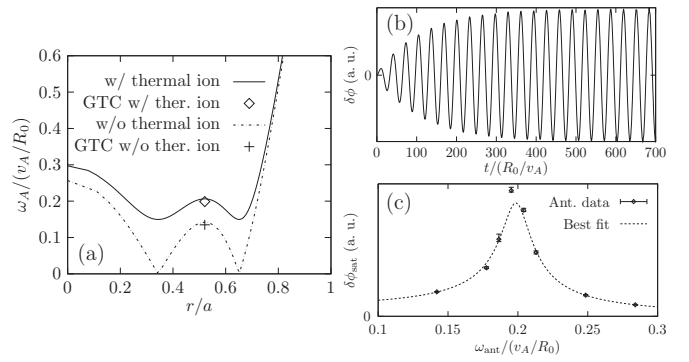


FIG. 4. Antenna excitation of  $n=4$ ,  $m=7$ , and  $l=0$  RSAE with kinetic thermal ions using GTC. (a)  $m=7$  Alfvén continua and eigenfrequencies obtained from GTC simulations with and without thermal ions. (b) Time history of electrostatic potential  $\delta\phi$  for antenna frequency  $\omega_{\text{ant}}=0.195v_A/R_0$  showing the saturation of the mode. (c) Saturated  $\delta\phi$  amplitude vs antenna frequency and best fit to estimate the RSAE damping rate.

Then simulations with kinetic thermal ions are investigated. In equilibrium, the thermal ions are protons with a Maxwellian velocity distribution and uniform temperature and density profiles with these on-axis parameters:  $v_i/v_A=0.08$ ,  $\rho_i/a=0.008$ , and  $k_{\theta}\rho_i=0.1$ . The drift-kinetic limit is taken for the thermal ions since  $k_{\theta}\rho_i \ll 1$ . The Alfvén continua are modified by the thermal ions as discussed at the end of Sec. II C. The  $m=7$  continuum calculated from Eq. (31) is plotted in Fig. 4(a) along with the continuum in the cold plasma limit for comparison. The kinetic thermal ions introduce the ion Landau damping, which causes the antenna excited mode to saturate. Since the antenna excitation of a wave is conceptually the same as a forced oscillator, the saturated wave amplitude is related to the RSAE damping rate by<sup>62</sup>

$$\delta\phi_{\text{sat}} \propto \frac{1}{\sqrt{(\omega_0^2 - \omega_{\text{ant}}^2)^2 + 4\gamma^2\omega_{\text{ant}}^2}}, \quad (32)$$

where  $\omega_0^2 = \omega_r^2 + \gamma^2$ ,  $\omega_r$  being the wave real frequency and  $\gamma$  being the wave damping rate. The saturated  $\delta\phi$  amplitude versus the antenna frequency is plotted in Fig. 4(c). Performing a best fit in Fig. 4(c) gives  $|\gamma|=0.0106v_A/R_0$  and  $\omega_r=0.199v_A/R_0$ . The damping rate can also be estimated by the simulation with an initial perturbation but no fast ion or antenna. Such a simulation in GTC gives  $|\gamma|=0.011v_A/R_0$  and  $\omega_r=0.198v_A/R_0$ , which is very close to the result from the antenna excitation for both real frequency and damping rate. Such a simulation in XHMGC gives  $|\gamma|=0.017v_A/R_0$  and  $\omega_r=0.218v_A/R_0$ , which is close to the GTC results for the frequency. The difference in the damping rate between the two codes could be due to the differences in geometry and parallel equilibrium current and the numerical dissipation in XHMGC.

#### IV. FAST ION EXCITATION OF RSAE

In our simulations, fast ions with a Maxwellian distribution are used with these on-axis parameters:  $v_f/v_A=0.3$ ,  $\rho_f/a=0.03$ ,  $k_{\perp}\rho_f=0.4$ , and  $n_{f0}/n_{e0}=0.01$ , where  $v_f$  is the fast ion thermal speed. At first, the drift-kinetic limit is taken for the fast ions for the purpose of benchmark, which is margin-

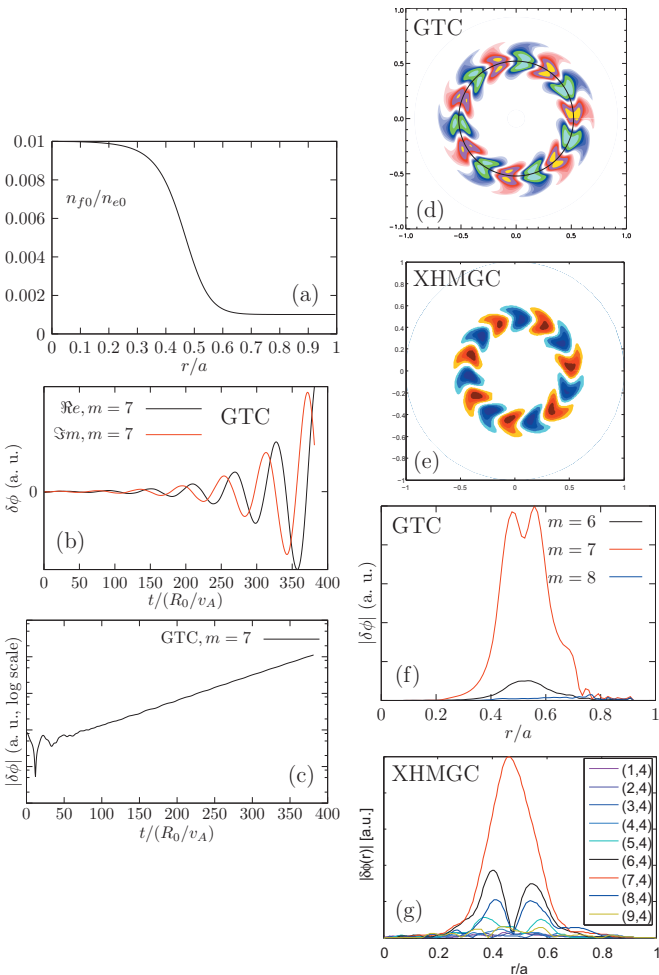


FIG. 5. (Color) Fast ion excitation of  $n=4$  and  $m=7$  RSAE without kinetic thermal ions using GTC and XHMGC. (a) Fast ion density profile. (b) Time history of electrostatic potential  $\delta\phi$ . (c) Time history of  $|\delta\phi|$  in logarithmic-linear plot. [(d) and (e)] Poloidal contour plots of  $\delta\phi$  from GTC and XHMGC, respectively. [(f) and (g)] Radial profiles of  $\delta\phi$   $m$ -harmonics from GTC and XHMGC, respectively.

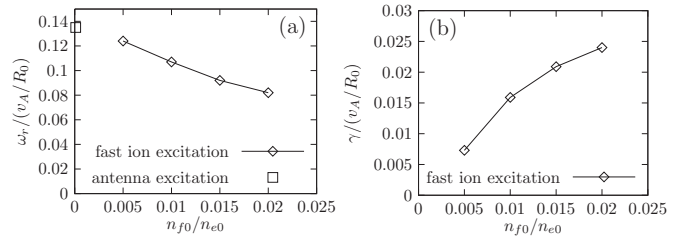


FIG. 7.  $m=7$  RSAE frequency and growth rate dependence on the fast ion density. (a) Frequency dependence on the fast ion density. (b) Growth rate dependence on the fast ion density.

ally good as  $k_{\perp}\rho_f \ll 1$  is barely satisfied. The case with the FLR effects is also studied. The fast ions have a uniform temperature and a nonuniform density profile shown in Fig. 5(a). The maximum density gradient is at the  $q_{\min}$  surface and its value is  $R_0/L_{n_f0} = 36.6$ . When kinetic thermal ions are not loaded, the  $m=7$  RSAE is driven unstable by the fast ions.

To avoid numerical errors, GTC convergence tests are done and the results are shown in Fig. 6. The spatial resolution convergence requires about 30 poloidal number of grids per wavelength. The time resolution convergence requires the time step to be smaller than  $0.1R_0/v_A$ . The results do not change much for the number of fast ion particles per cell ranging from 10 to 100. The frequencies from the two codes are  $\omega_{\text{GTC}} = 0.107v_A/R_0$  and  $\omega_{\text{XHMGC}} = 0.145v_A/R_0$ , respectively. The growth rates are  $\gamma_{\text{GTC}} = 0.0159v_A/R_0$  and  $\gamma_{\text{XHMGC}} = 0.013v_A/R_0$ . The growth rates from the two codes are quite close, while the discrepancy between the frequencies is larger. To confirm that this mode is still a RSAE with such a frequency difference, we perform simulations with various densities of the fast ions to examine the corresponding frequency and growth rate change as shown in Fig. 7. It can be seen from the results that when the fast ion density goes to 0, the growth rate goes to 0 and the frequency goes to

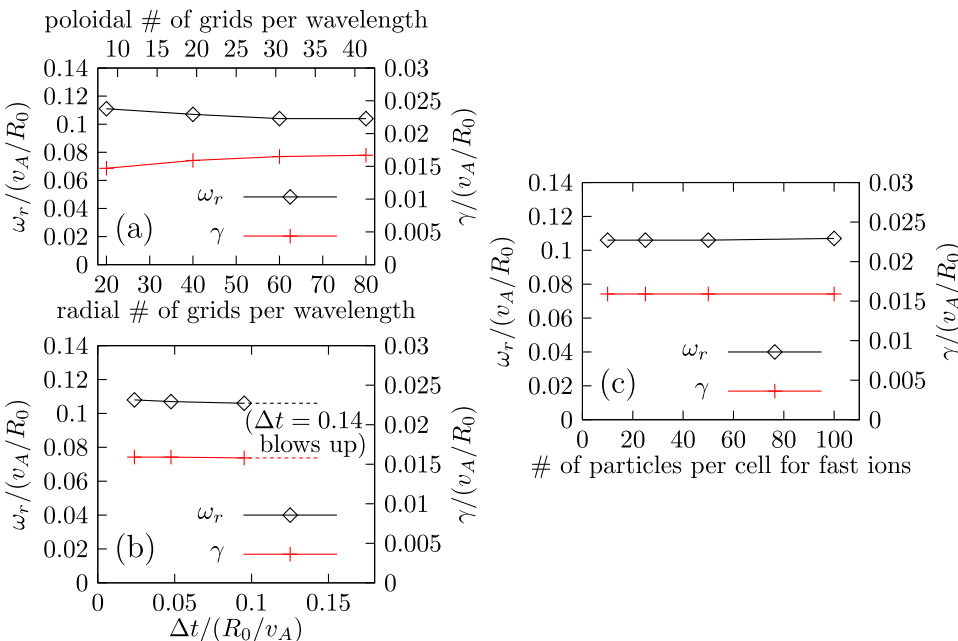


FIG. 6. (Color online) Convergence tests for  $n=4$  and  $m=7$  RSAE excited by fast ions but without kinetic effects of thermal ions. Mode frequency and growth rate depending on (a) number of grids per wavelength, (b) time step size, and (c) fast ion number of particles per cell.

TABLE I. Frequency and growth rate comparison of the  $n=4$  and  $m=7$  RSAE without thermal ions between GTC and XHMGC.

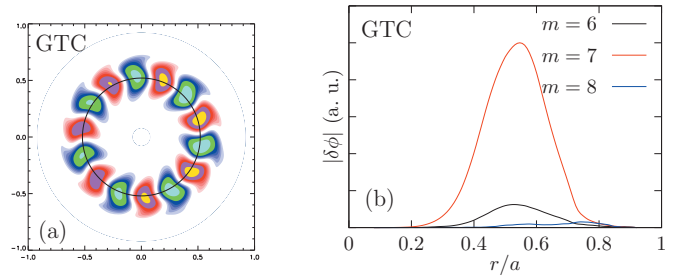
Unit: $v_A/R_0$	GTC	XHMGC
Ideal MHD accumulation point	$\omega_r=0.142$	
Antenna excitation (no fast ion)	$\omega_r=0.135$	$\omega_r=0.160$
Antenna excitation (uniform $n_{f0}$ )	$\omega_r=0.134$	$\omega_r=0.160$
Fast ion excitation (nonuniform $n_{f0}$ , without FLR effects)	$\omega_r=0.107$ $\gamma=0.0159$	$\omega_r=0.145$ $\gamma=0.013$
Fast ion excitation (nonuniform $n_{f0}$ , with FLR effects)	$\omega_r=0.108$ $\gamma=0.0090$	Did not do this case

the one obtained by antenna excitation and by initial perturbation. Also, the real frequency change and the growth rate change by the fast ions are of the same order of magnitude, confirming that the fast ion excited mode is the  $m=7$  RSAE. The mode structures from the two codes are similar as shown in Figs. 5(d)–5(g), except that the mode structure from GTC shows a little dip near  $q_{\min}$ . This may be formed by the coexistence of some higher radial harmonics in addition to the zeroth radial harmonic. Compared to the ellipselike mode structure obtained in antenna excitation in Figs. 2(b) and 2(c), it can be seen from Figs. 5(d) and 5(e) that the mode structure is modified to be triangle-like by the nonperturbative contribution of the fast ions. This phenomenon has also recently been observed in Toroidal Alfvén Eigenmode Gyrofluid (TAEFL) simulations and DIII-D experiments.<sup>63</sup> The mode structure change is due to the radial symmetry breaking by the variation of the fast ion density gradient. When the FLR effects are included, the frequency and mode structure have no significant change, while the growth rate is lowered by about 43%.

Table I summarizes the comparisons between GTC and XHMGC of frequency and growth rate for the antenna excitation and the fast ion excitation. The two rows of the antenna excitation show that uniform fast ions have almost no effect on the frequency in both codes. The last two rows show that nonuniform fast ions reduce the mode frequency. The frequency is lowered by about 21% in GTC and about 9% in XHMGC. This part of the discrepancy is probably due to the differences of the fast ion formulation and the geometry model, as well as the parallel equilibrium current.

TABLE II. Frequency and growth rate comparison of the  $n=4$  and  $m=7$  RSAE with thermal ions between GTC and XHMGC.

Unit: $v_A/R_0$	GTC	XHMGC
Theoretical accumulation point	$\omega=0.206$	
Antenna excitation (no fast ion)	$\omega_r=0.199$ $\gamma=-0.0106$	$\omega_r=0.207$
Initial perturbation (no fast ion)	$\omega_r=0.198$ $\gamma=-0.011$	$\omega_r=0.218$ $\gamma=-0.017$
Fast ion excitation (without FLR effects)	$\omega_r=0.168$ $\gamma=0.0174$	No growth for $n_{f0}/n_{e0}=0.01$
Fast ion excitation (with FLR effects)	$\omega_r=0.171$ $\gamma=0.0087$	Did not do this case

FIG. 8. (Color) Fast ion excitation of  $n=4$ ,  $m=7$  RSAE with kinetic thermal ions using GTC. (a) Poloidal contour plot of  $\delta\phi$ . (b) Radial profiles of  $\delta\phi$   $m$ -harmonics.

When kinetic thermal ions are added in, the charge neutrality condition is strictly enforced. The frequency and the growth rate from GTC are  $\omega_{\text{GTC}}=0.168v_A/R_0$  and  $\gamma_{\text{GTC}}=0.0174v_A/R_0$ , respectively. The XHMGC simulation shows no growth for this fast ion density. For a larger fast ion density, XHMGC does show the RSAE with an exponential growth. The fact that the growth rate in GTC is larger than that in XHMGC may be due to the numerical dissipation from the finite resistivity in XHMGC. The comparison of the frequencies for the case with kinetic thermal ions is summarized in Table II. For the antenna excitation, the mode structure has no significant change. For the fast ion excitation, the mode structure has some change by the kinetic thermal ions as shown in Fig. 8.

## V. SUMMARY

Global gyrokinetic particle simulations of RSAE have been successfully performed and verified. We have excited the RSAE by initial perturbation, by external antenna, and by energetic ions. The RSAE excitation by antenna provides verifications of the mode structure, the frequency, and the damping rate. When the kinetic effects of the background plasma are artificially suppressed, the mode amplitude shows a near-linear growth. With kinetic thermal ions, the mode amplitude eventually saturates due to the thermal ion damping. The damping rates measured from the antenna excitation and from the initial perturbation simulation agree very well. The RSAE excited by fast ions shows an exponential growth. The finite Larmor radius effects of the fast ions are found to significantly reduce the growth rate. With kinetic thermal ions and electron pressure, the mode frequency increases due to the elevation of the Alfvén continuum by the geodesic compressibility. The nonperturbative contributions from the fast ions and kinetic thermal ions modify the mode structure relative to the ideal MHD theory. The gyrokinetic simulations have been benchmarked with extended hybrid MHD-gyrokinetic simulations.

## ACKNOWLEDGMENTS

We acknowledge useful discussions with L. Chen, M. Van Zeeland, H.S. Zhang, and F. Zonca. We thank the referee for pointing out the effects of neglecting parallel equilibrium current in the current GTC simulations. This work was sup-

ported by the U.S. Department of Energy (DOE) SciDAC GSEP center. Simulations were performed using supercomputers at NERSC and ORNL.

- <sup>1</sup>C. Z. Cheng, L. Chen, and M. S. Chance, *Ann. Phys.* **161**, 21 (1985).
- <sup>2</sup>H. L. Berk, D. N. Borba, B. N. Breizman, S. D. Pinches, and S. E. Sharapov, *Phys. Rev. Lett.* **87**, 185002 (2001).
- <sup>3</sup>L. Chen, *Phys. Plasmas* **1**, 1519 (1994).
- <sup>4</sup>H. Kimura, Y. Kusama, M. Saigusa, G. Kramer, K. Tobita, M. Nemoto, T. Kondoh, T. Nishitani, O. D. Costa, T. Ozeki, T. Oikawa, S. Moriyama, A. Morioka, G. Fu, C. Cheng, and V. Afanas'ev, *Nucl. Fusion* **38**, 1303 (1998).
- <sup>5</sup>S. E. Sharapov, D. Testa, B. Alper, D. N. Borba, A. Fasoli, N. C. Hawkes, R. F. Heeter, M. Mantsinen, and M. G. Von Hellermann, *Phys. Lett. A* **289**, 127 (2001).
- <sup>6</sup>R. Nazikian, G. J. Kramer, C. Z. Cheng, N. N. Gorelenkov, H. L. Berk, and S. E. Sharapov, *Phys. Rev. Lett.* **91**, 125003 (2003).
- <sup>7</sup>J. A. Snipes, N. Basse, C. Boswell, E. Edlund, A. Fasoli, N. N. Gorelenkov, R. S. Granetz, L. Lin, Y. Lin, R. Parker, M. Porkolab, J. Sears, S. Sharapov, V. Tang, and S. Wukitch, *Phys. Plasmas* **12**, 056102 (2005).
- <sup>8</sup>M. A. Van Zeeland, G. J. Kramer, R. Nazikian, H. L. Berk, T. N. Carlstrom, and W. M. Solomon, *Plasma Phys. Controlled Fusion* **47**, L31 (2005).
- <sup>9</sup>E. D. Fredrickson, N. A. Crocker, N. N. Gorelenkov, W. W. Heidbrink, S. Kubota, F. M. Levinton, H. Yuh, J. E. Menard, and R. E. Bell, *Phys. Plasmas* **14**, 102510 (2007).
- <sup>10</sup>F. Zonca, L. Chen, and R. A. Santoro, *Plasma Phys. Controlled Fusion* **38**, 2011 (1996).
- <sup>11</sup>F. Zonca, L. Chen, J. Q. Dong, and R. A. Santoro, *Phys. Plasmas* **6**, 1917 (1999).
- <sup>12</sup>R. Nazikian, H. L. Berk, R. V. Budny, K. H. Burrell, E. J. Doyle, R. J. Fonck, N. N. Gorelenkov, C. Holcomb, G. J. Kramer, R. J. Jayakumar, R. J. L. Haye, G. R. McKee, M. A. Makowski, W. A. Peebles, T. L. Rhodes, W. M. Solomon, E. J. Strait, M. A. VanZeeland, and L. Zeng, *Phys. Rev. Lett.* **96**, 105006 (2006).
- <sup>13</sup>L. Chen and F. Zonca, *Nucl. Fusion* **47**, S727 (2007).
- <sup>14</sup>S. E. Sharapov, B. Alper, J. Fessey, N. C. Hawkes, N. P. Young, R. Nazikian, G. J. Kramer, D. N. Borba, S. Hacquin, E. De La Luna, S. D. Pinches, J. Rapp, D. Testa, and JET-EFDA Contributors, *Phys. Rev. Lett.* **93**, 165001 (2004).
- <sup>15</sup>M. Van Zeeland, M. Austin, T. Carlstrom, T. Deterly, D. Finkenthal, C. Holcomb, R. Jayakumar, G. Kramer, M. Makowski, G. McKee, R. Nazikian, W. Peebles, T. Rhodes, W. Solomon, and E. Strait, *Nucl. Fusion* **46**, S880 (2006).
- <sup>16</sup>E. Joffrin, G. Gorini, C. D. Challis, N. C. Hawkes, T. C. Hender, D. F. Howell, P. Maget, P. Mantica, D. Mazon, S. E. Sharapov, G. Tresset, and contributors to the EFDA-JET Work programme, *Plasma Phys. Controlled Fusion* **44**, 1739 (2002).
- <sup>17</sup>E. Joffrin, C. D. Challis, G. D. Conway, X. Garbet, A. Gude, S. Günter, N. C. Hawkes, T. C. Hender, D. F. Howell, G. T. A. Huysmans, E. Lazzaro, P. Maget, M. Maracheq, A. G. Peeters, S. D. Pinches, S. E. Sharapov, and JET-EFDA Contributors, *Nucl. Fusion* **43**, 1167 (2003).
- <sup>18</sup>A. Marinoni, P. Mantica, D. Van Eester, F. Imbeaux, M. Mantsinen, N. Hawkes, E. Joffrin, V. Kiptily, S. D. Pinches, A. Salmi, S. Sharapov, I. Voitsekhovitch, P. de Vries, K. D. Zastrow, and JET-EFDA Contributors, *Plasma Phys. Controlled Fusion* **48**, 1469 (2006).
- <sup>19</sup>S. E. Sharapov, B. Alper, Yu. F. Baranov, H. L. Berk, D. Borba, C. Boswell, B. N. Breizman, C. D. Challis, M. de Baar, E. De La Luna, E. A. Evangelidis, S. Hacquin, N. C. Hawkes, V. G. Kiptily, S. D. Pinches, P. Sandquist, I. Voitsekhovich, N. P. Young, and JET-EFDA Contributors, *Nucl. Fusion* **46**, S868 (2006).
- <sup>20</sup>M. W. Shafer, G. R. McKee, M. E. Austin, K. H. Burrell, R. J. Fonck, and D. J. Schlossberg, *Phys. Rev. Lett.* **103**, 075004 (2009).
- <sup>21</sup>H. Smith, B. N. Breizman, M. Lisak, and D. Anderson, *Phys. Plasmas* **13**, 042504 (2006).
- <sup>22</sup>M. A. Van Zeeland, M. E. Austin, N. N. Gorelenkov, W. W. Heidbrink, G. J. Kramer, M. A. Makowski, G. R. McKee, R. Nazikian, E. Ruskov, and A. D. Turnbull, *Phys. Plasmas* **14**, 056102 (2007).
- <sup>23</sup>F. Zonca, S. Briguglio, L. Chen, S. Dettrick, G. Fogaccia, D. Testa, and G. Vlad, *Phys. Plasmas* **9**, 4939 (2002).
- <sup>24</sup>B. N. Breizman, H. L. Berk, M. S. Pekker, S. D. Pinches, and S. E. Sharapov, *Phys. Plasmas* **10**, 3649 (2003).
- <sup>25</sup>M. Takechi, A. Fukuyama, M. Ishikawa, C. Z. Cheng, K. Shinohara, T. Ozeki, Y. Kusama, S. Takeji, T. Fujita, T. Oikawa, T. Suzuki, N. Oyama, A. Morioka, N. N. Gorelenkov, G. J. Kramer, and R. Nazikian, *Phys. Plasmas* **12**, 082509 (2005).
- <sup>26</sup>M. A. Van Zeeland, W. W. Heidbrink, R. Nazikian, W. M. Solomon, M. E. Austin, H. L. Berk, N. N. Gorelenkov, C. T. Holcomb, A. W. Hyatt, G. J. Kramer, J. Lohr, M. A. Makowski, G. R. McKee, C. C. Petty, S. E. Sharapov, and T. L. Rhodes, *Plasma Phys. Controlled Fusion* **50**, 035009 (2008).
- <sup>27</sup>G. J. Kramer and G.-Y. Fu, *Plasma Phys. Controlled Fusion* **48**, 1285 (2006).
- <sup>28</sup>G. J. Kramer, N. N. Gorelenkov, R. Nazikian, and C. Z. Cheng, *Plasma Phys. Controlled Fusion* **46**, L23 (2004).
- <sup>29</sup>B. N. Breizman, M. S. Pekker, and S. E. Sharapov, *Phys. Plasmas* **12**, 112506 (2005).
- <sup>30</sup>G. Y. Fu and H. L. Berk, *Phys. Plasmas* **13**, 052502 (2006).
- <sup>31</sup>N. N. Gorelenkov, G. J. Kramer, and R. Nazikian, *Plasma Phys. Controlled Fusion* **48**, 1255 (2006).
- <sup>32</sup>S. V. Konovalov, A. B. Mikhailovskii, M. S. Shirokov, E. A. Kovalishen, and T. Ozeki, *Phys. Plasmas* **11**, 4531 (2004).
- <sup>33</sup>N. N. Gorelenkov, *Phys. Plasmas* **15**, 110701 (2008).
- <sup>34</sup>F. Zonca and L. Chen, *Plasma Phys. Controlled Fusion* **48**, 537 (2006).
- <sup>35</sup>L. Yu, G.-Y. Fu, and Z.-M. Sheng, *Phys. Plasmas* **16**, 072505 (2009).
- <sup>36</sup>G. Vlad, S. Briguglio, G. Fogaccia, F. Zonca, and M. Schneider, *Nucl. Fusion* **46**, 1 (2006).
- <sup>37</sup>P. Lauber, S. Gunter, and S. D. Pinches, *Phys. Plasmas* **12**, 122501 (2005).
- <sup>38</sup>Y. Nishimura, Z. Lin, and W. X. Wang, *Phys. Plasmas* **14**, 042503 (2007).
- <sup>39</sup>Y. Nishimura, *Phys. Plasmas* **16**, 030702 (2009).
- <sup>40</sup>A. Mishchenko, A. Konies, and R. Hatzky, *Phys. Plasmas* **16**, 082105 (2009).
- <sup>41</sup>J. Lang, Y. Chen, S. E. Parker, and G.-Y. Fu, *Phys. Plasmas* **16**, 102101 (2009).
- <sup>42</sup>E. M. Bass and R. E. Waltz, "Gyrokinetic simulations of mesoscale energetic particle driven Alfvénic turbulent transport embedded in microturbulence," *Phys. Plasmas* (in press).
- <sup>43</sup>Z. Lin, T. S. Hahm, W. W. Lee, W. M. Tang, and R. B. White, *Science* **281**, 1835 (1998).
- <sup>44</sup>I. Holod, W. L. Zhang, Y. Xiao, and Z. Lin, *Phys. Plasmas* **16**, 122307 (2009).
- <sup>45</sup>Y. Nishimura, Z. Lin, and L. Chen, *Comm. Comp. Phys.* **5**, 183 (2009).
- <sup>46</sup>Y. Xiao and Z. Lin, *Phys. Rev. Lett.* **103**, 085004 (2009).
- <sup>47</sup>W. Deng and Z. Lin, *Phys. Plasmas* **16**, 102503 (2009).
- <sup>48</sup>W. Zhang, Z. Lin, and L. Chen, *Phys. Rev. Lett.* **101**, 095001 (2008).
- <sup>49</sup>H. S. Zhang, Z. Lin, I. Holod, X. Wang, Y. Xiao, and W. L. Zhang, "Gyrokinetic particle simulations of beta-induced Alfvén eigenmode," *Phys. Plasmas* (in press).
- <sup>50</sup>A. Fasoli, D. Borba, G. Bosia, D. J. Campbell, J. A. Dobbing, C. Gormezano, J. Jacquinet, P. Lavanchy, J. B. Lister, P. Marmillod, J.-M. Moret, A. Santagiustina, and S. Sharapov, *Phys. Rev. Lett.* **75**, 645 (1995).
- <sup>51</sup>A. Fasoli, D. Testa, T. Panis, A. Klein, J. A. Snipes, J. Sears, M. Gryaznevich, R. Martin, S. D. Pinches, and JET-EFDA Contributors, *Plasma Phys. Controlled Fusion* **52**, 075015 (2010).
- <sup>52</sup>X. Wang, F. Zonca, and L. Chen, *Plasma Phys. Controlled Fusion* **52**, 115005 (2010).
- <sup>53</sup>X. Wang, A. Bierwage, S. Briguglio, L. Chen, G. Fogaccia, G. Vlad, C. D. Troia, F. Zonca, H. Zhang, and Z. Lin, Proceedings of the 23rd IAEA Fusion Energy Conference, Daejeon, Korea, 10–16 October 2010, Paper No. THW/2–4Ra.
- <sup>54</sup>A. J. Brizard and T. S. Hahm, *Rev. Mod. Phys.* **79**, 421 (2007).
- <sup>55</sup>Z. Lin and L. Chen, *Phys. Plasmas* **8**, 1447 (2001).
- <sup>56</sup>Z. Lin, Y. Nishimura, Y. Xiao, I. Holod, W. L. Zhang, and L. Chen, *Plasma Phys. Controlled Fusion* **49**, B163 (2007).
- <sup>57</sup>W. Lee, *J. Comput. Phys.* **72**, 243 (1987).
- <sup>58</sup>W. Park, S. Parker, H. Biglari, M. Chance, L. Chen, C. Z. Cheng, T. S. Hahm, W. W. Lee, R. Kulsrud, D. Monticello, L. Sugiyama, and R. White, *Phys. Fluids B* **4**, 2033 (1992).
- <sup>59</sup>M. Van Zeeland, W. Heidbrink, R. Nazikian, M. Austin, C. Cheng, M. Chu, N. Gorelenkov, C. Holcomb, A. Hyatt, G. Kramer, J. Lohr, G. McKee, C. Petty, R. Prater, W. Solomon, and D. Spong, *Nucl. Fusion* **49**, 065003 (2009).

<sup>60</sup>M. S. Chu, J. M. Greene, L. L. Lao, A. D. Turnbull, and M. S. Chance, *Phys. Fluids B* **4**, 3713 (1992).

<sup>61</sup>S. Briguglio, F. Zonca, and G. Vlad, *Phys. Plasmas* **5**, 3287 (1998).

<sup>62</sup>J. Harris, W. Benenson, and H. Stöcker, *Handbook of Physics*, edited by J. Harris, W. Benenson, and H. Stöcker (Springer, New York, 2002).

<sup>63</sup>B. Tobias, I. G. J. Classen, C. W. Domier, W. W. Heidbrink, N. C. Luhmann, Jr., R. Nazikian, H. K. Park, D. Spong, and M. A. Van Zeeland, "Fast ion induced shearing of 2-D Alfvén eigenmodes measured by electron cyclotron emission imaging," *Phys. Rev. Lett.* (submitted).